NASA TECHNICAL NOTE

NASA TN D-7819

NASA TN D-7819

FLIGHT-DETERMINED LAG OF ANGLE-OF-ATTACK AND ANGLE-OF-SIDESLIP SENSORS IN THE YF-12A AIRPLANE FROM ANALYSIS OF DYNAMIC MANEUVERS

by Glenn B. Gilyard and Daumants Belte

Flight Research Center
Edwards, Calif. 93523

NATIONAL AERONAUTICS AND SPACE ADMINISTRATION • WASHINGTON, D. C. • OCTOBER 1974

FLIGHT-DETERMINED LAG OF ANGLE-OF-ATTACK AND

ANGLE-OF-SIDESLIP SENSORS IN THE YF-12A AIRPLANE

FROM ANALYSIS OF DYNAMIC MANEUVERS

Glenn B. Gilyard and Daumants Belte
Flight Research Center

INTRODUCTION

The high temperature environment of cruise flight near Mach 3 makes vane-type flow direction sensors generally inadequate for use on the YF-12 aircraft. As a result, angle of attack and angle of sideslip are measured by a fixed four-port pressure-sensing hemispherical head mounted on the nose boom. The presence of time lag errors in pitot-static instrumentation is documented in references 1 to 3, in which it is noted that the lag can be as great as several seconds at high altitudes and airspeeds. Less attention has been paid to lag in angle-of-attack and angle-of-sideslip pressure sensors. The lag of these sensors is considerably less than that in pitot-static systems; however, a small lag in the measurement of angle of attack and angle of sideslip can be critical when these variables are used in stability derivative determination or as inputs to a control system. For example, in the YF-12 flight program, a lag in the sideslip angle sensed by the inlet control system caused the inlet forward bypass door to drive the vehicle unstable (ref. 4) when the stability augmentation system (SAS) was switched off.

Theoretically lag has been determined by computing estimates based on viscous lag theory (as in ref. 2) and experimentally by applying known pressure variations to the instrument pressure ports in laboratory ground tests. This report presents three other methods of determining lag from dynamic stability and control maneuver data: time vector, Newton-Raphson, and least squares. Lags of the YF-12A angle-of-attack and angle-of-sideslip sensor systems are documented throughout the flight envelope, and the results are compared with those obtained by using viscous lag theory.

SYMBOLS

Physical quantities in this report are given in the International System of Units (SI) and parenthetically in U.S. Customary Units. The measurements were taken in U.S. Customary Units. Factors relating the two systems are presented in reference 5.

a_n normal acceleration at center of gravity, g units

a_t transverse acceleration at center of gravity, g units

g acceleration due to gravity, meters/second^2 (feet/second^2)

h pressure altitude, meters (feet)

I_X, I_Y, I_Z moment of inertia about the X-, Y-, and Z-body axes, respectively, kilogram-meter^2 (slug-foot^2)

I_{XZ} product of inertia referred to the X- and Z-body axes, kilogram-meter^2 (slug-foot^2)

K empirical constant coefficient of the pneumatic lag equation

$L_y = \dfrac{1}{I_X} \dfrac{\partial \text{Rolling moment}}{\partial y}$ where $y = \beta$, p, r, δ_a, or δ_r

M Mach number

$M_z = \dfrac{1}{I_Y} \dfrac{\partial \text{Pitching moment}}{\partial z}$ where $z = \alpha$, q, or δ_e

$N_y = \dfrac{1}{I_Z} \dfrac{\partial \text{Yawing moment}}{\partial y}$ where $y = \beta$, p, r, δ_a, or δ_r

$N_z = \dfrac{1}{(\text{Aircraft mass})(V)} \dfrac{\partial \text{Normal force}}{\partial z}$ where $z = \alpha$, q, or δ_e

P pressure, newtons/meter^2 (pounds/foot^2)

p, q, r roll, pitch, and yaw rate, respectively, radians/second (unless otherwise noted)

$\bar{q}$ dynamic pressure, newtons/meter^2 (pounds/foot^2)

s Laplace operator

T temperature, degrees Kelvin (Rankine)

t time, seconds

V velocity, meters/second (feet/second)

x_α, x_β distance from center of gravity to angle-of-attack and angle-of-sideslip sensor, respectively, positive forward, meters (feet)

2

$$Y_y = \frac{1}{(\text{Aircraft mass})(V)} \frac{\partial \text{Side force}}{\partial y} \quad \text{where} \quad y = \beta, \ p, \ r, \ \delta_a, \ \text{or} \ \delta_r$$

α	angle of attack at center of gravity, radians (unless otherwise noted)
β	angle of sideslip at center of gravity, radians (unless otherwise noted)
γ	ratio of specific heats, 1.4 for air
Δ	incremental change
$\Delta P_\alpha, \Delta P_\beta$	differential pressure measured by the sensor in the α and β plane, respectively, newtons/meter^2 (pounds/foot^2)
$\delta_a, \delta_e, \delta_r$	aileron, elevator, and rudder deflection, respectively, radians (unless otherwise noted), positive when aileron deflection produces right roll, elevator trailing edge down, trailing edge of rudder left
ζ	damping ratio
θ, φ	Euler angle of pitch and roll, respectively, radians (unless otherwise noted)
μ	coefficient of viscosity, newtons-second/meter^2 (pounds-second/foot^2)
σ	standard deviation
τ	time constant, seconds
Φ_d	damping angle, $\sin^{-1}(\zeta)$, degrees
$\Phi_{j/k}$	phase angle of quantity j relative to quantity k, degrees
ω_d, ω_n	damped and undamped natural frequency of the airplane in oscillation, respectively, radians/second

Subscripts:

c	calculated
f	flight
i	indicated
o	initial

t_2 stagnation condition

∞ free-stream condition

45°   angle of the α and β ports on the hemispherical head with respect to the centerline of the probe, degrees

θ port angle from centerline of hemispherical head

A dot over a quantity denotes the time derivative of that quantity.

AIRPLANE AND INSTRUMENTATION

The YF-12A airplane (ref. 4) is a twin-engined, delta-winged interceptor designed for sustained cruise above Mach 3 and altitudes greater than 24,400 meters (80,000 feet). As noted previously, the high temperature environment of Mach 3 cruise flight necessitated the use of a fixed four-port pressure sensing hemispherical head to obtain angle-of-attack and angle-of-sideslip measurements on the airplane. Reference 6 describes the α-β sensor and its calibration in detail. The sensor, attached as a dogleg to the nose boom probe, is shown on the airplane in figure 1.
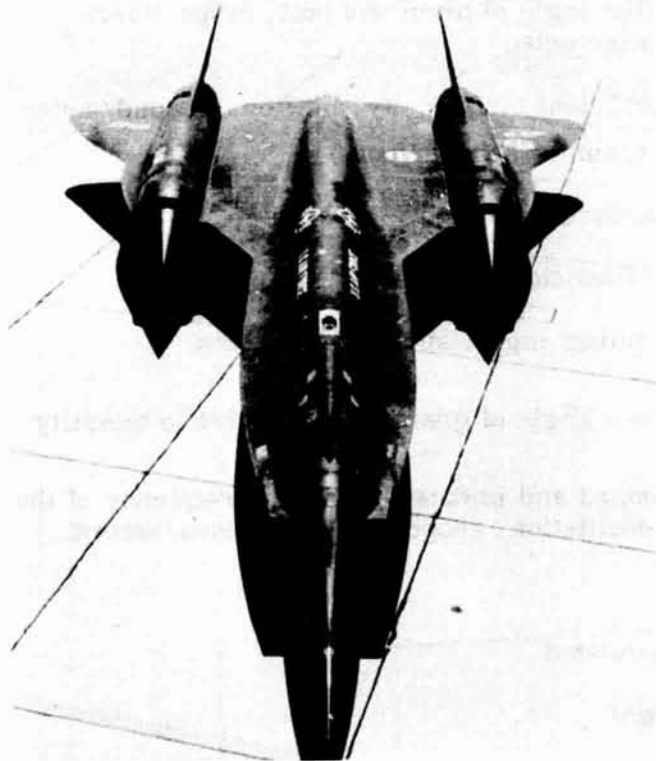

Figure 1.   Test airplane with nose boom probe attached.   E-23131

4

A closeup of the assembly is shown in figure 2, and a dimensioned three-view drawing in figure 3.
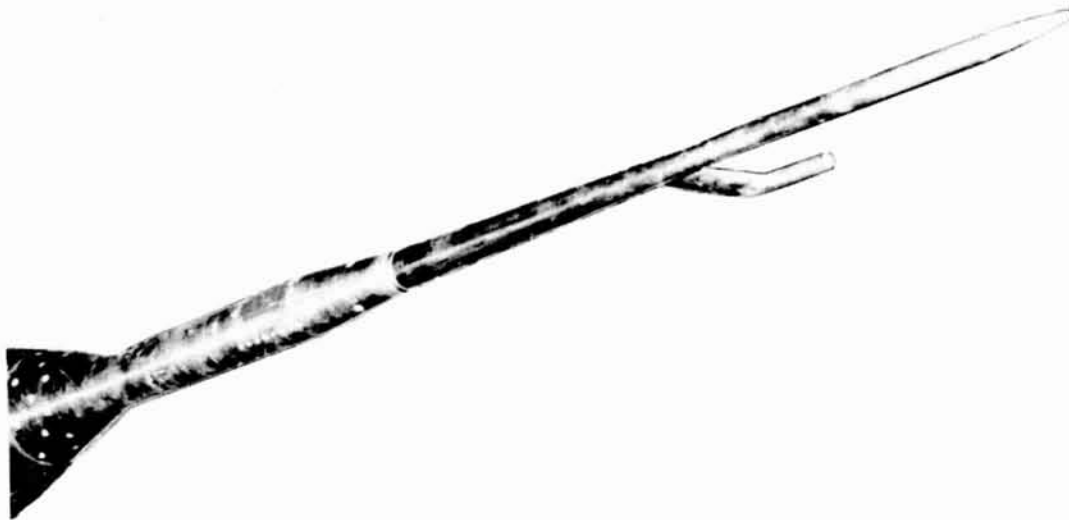

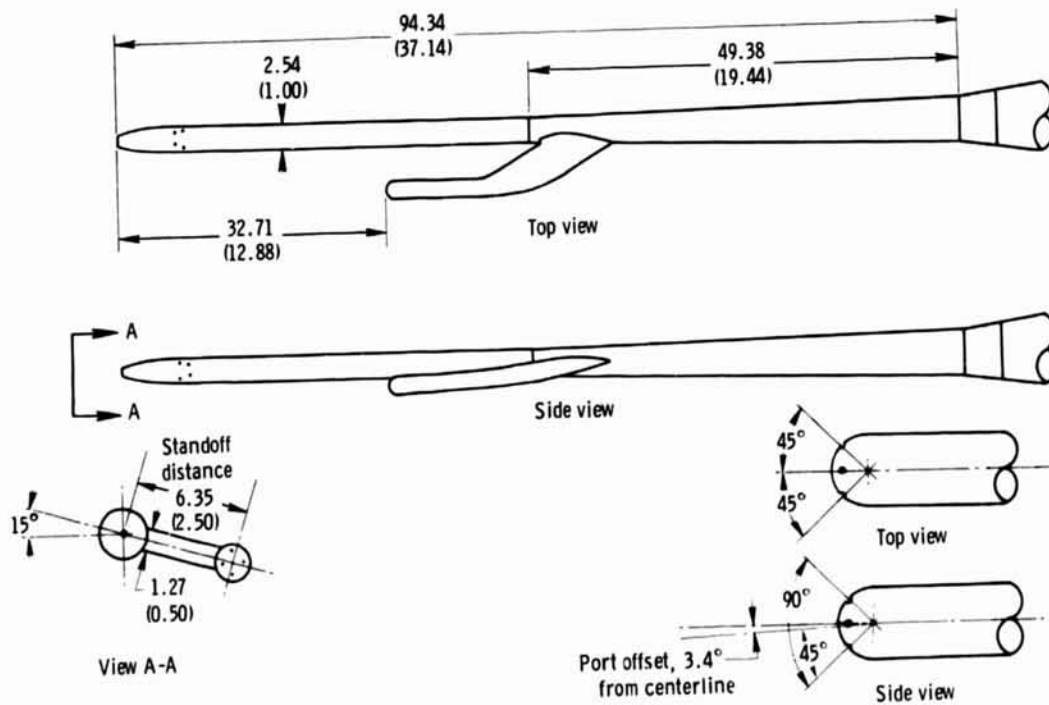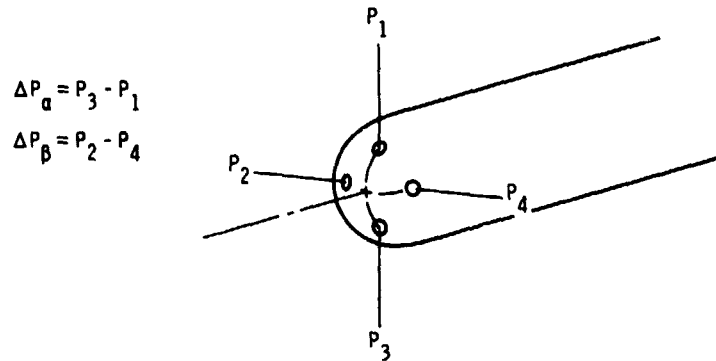Figure 2. Closeup of nose boom probe showing the α-β sensor assembly.

E-23909

Figure 3. Nose boom probe dimensions (in centimeters (inches)) with details of sensor head configuration.

Basically, the $\alpha-\beta$ sensor provides differential pressures, ΔP_α and ΔP_β, as shown in the following sketch:

$$\Delta P_\alpha = P_3 - P_1$$

$$\Delta P_\beta = P_2 - P_4$$

The sensor is connected to pressure transducers in the nose cone of the airplane. Geometric characteristics of the system are shown in the following schematic drawing and tabulation:

	Sensor system	
	α	β
Port —		
Depth, cm (in.)	0.203 (0.080)	0.203 (0.080)
Inside diameter, cm (in.)	0.178 (0.070)	0.178 (0.070)
Tubing —		
First segment:		
Length, cm (in.)	43.2 (17)	43.2 (17)
Inside diameter, cm (in.)	0.365 (0.144)	0.365 (0.144)
Second segment:		
Length, cm (in.)	640 (252)	640 (252)
Inside diameter, cm (in.)	0.493 (0.194)	0.493 (0.194)
Transducer volume —		
α or β pulse code modulation (PCM) instrumentation transducer, cm^3 (in^3)	16.4 (1)	16.4 (1)
Sum of remaining transducers used for onboard systems, cm^3 (in^3)	239.2 (14.6)	157.3 (9.6)
Total	255.6 (15.6)	173.7 (10.6)

Wind-tunnel calibration curves of $(\Delta P_\alpha/\bar{q})/\alpha$ and $(\Delta P_\beta/\bar{q})/\beta$ as a function of Mach number for this probe were obtained from reference 6 and are shown in figure 4. These curves were applied to the $\Delta P_\alpha/\bar{q}$ and $\Delta P_\beta/\bar{q}$ flight data to obtain

values of α and β as a function of time. For the maneuver analyses, dynamic pressure was assumed to be constant and was calculated from the initial Mach number and altitude conditions.
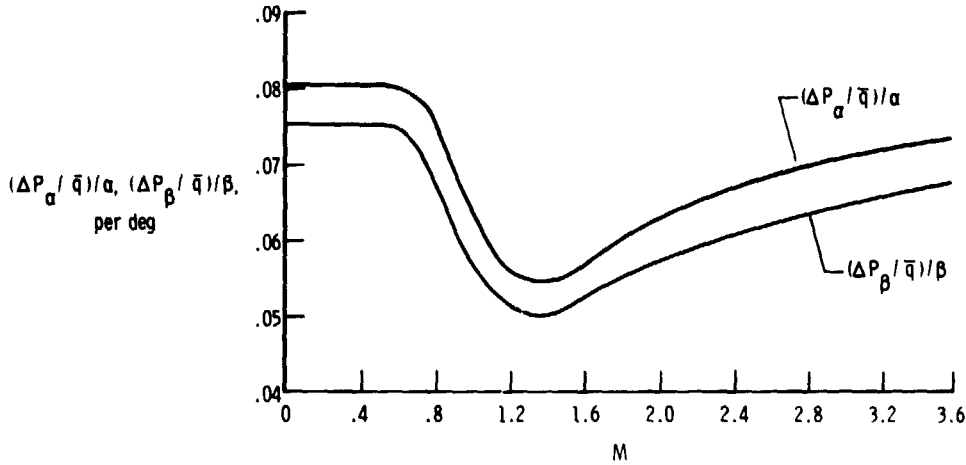

Figure 4. Calibration curves for conversion of differential pressures to angle-of-attack and angle-of-sideslip values as a function of Mach number. (Adapted from ref. 6.)

Basic stability and control instrumentation provided angular rates, normal and lateral accelerations, and pitch and roll attitudes.

Pertinent characteristics of the PCM system instrumentation used for the time lag analysis are listed in the following tabulation:

Parameter	System range	System resolution	ω_n, rad/sec
Pressure, P	$\pm 20,261$ N/m^2	79 N/m^2	3600
	$(\pm 424$ lb/ft$^2)$	$(1.65$ lb/ft$^2)$	
Roll rate, p	± 20 deg/sec	0.078 deg/sec	300
Pitch rate, q	± 10 deg/sec	0.039 deg/sec	150
Yaw rate, r	± 10 deg/sec	0.039 deg/sec	150
Euler angle of roll, φ	$\pm 60°$	0.234°	----
Euler angle of pitch, θ	$-15°, 25°$	0.078°	----
Normal acceleration, a_n	$-1g, 3g$	0.0078g	500
Transverse acceleration, a_t	$\pm 0.5g$	0.0020g	500

Data were recorded on magnetic tape by means of the PCM system and were analyzed at a rate of 40 points per second.

TEST MANEUVERS

The data used in this analysis were obtained in a previous study for which standard stability and control maneuvers were performed. Longitudinal data were

7

from elevator pulses, and lateral-directional data were from rudder and aileron doublets. The stability augmentation system was not used during the maneuvers so that damping would be as low as possible.

DATA ANALYSIS

Three methods of analysis were used to determine the lag of the α and β systems: time vector, Newton-Raphson, and least squares. For the purpose of this report, the α and β sensor systems are considered to include the probe, the tubing, the transducers, and the data acquisition system.

The time-vector method is suitable for use in analyzing free-oscillation maneuvers with damping ratios less than 0.3. Time histories calculated with the Newton-Raphson technique can be used to define lags for maneuvers that are oscillatory but not necessarily completely free of control inputs. The least-squares method, the most general of the three, is not restricted by high damping ratios or control inputs. With all three methods, the lag was determined by comparing flight data with calculated time histories.

Time-Vector Method

The time-vector method (ref. 7) establishes amplitude ratio and phase angle relationships between the different parameters in the linearized equations of motion. By using the appropriate vector format equations, shown in appendix A, phase relationships of α and β to other flight variables can be established without using α and β.

For a longitudinal maneuver (fig. 5) with pitch rate, q, and normal acceleration, a_n, available, the phase angle, $\Phi_{(\alpha_i/q)_c}$, can be calculated. The lag in the indicated α shows up as the discrepancy between this computed angle and the flight data, $\Phi_{(\alpha_i/q)_f}$.

For a lateral-directional maneuver, a similar procedure using roll rate, p, yaw rate, r, and transverse acceleration, a_t, produces a calculated $\Phi_{(\beta_i/r)_c}$. The difference in phasing between the calculated data and the flight data, $\Phi_{(\beta_i/r)_f}$, can be attributed to the lag in the indicated β.

The requirements of low damping and free oscillation limit the number of maneuvers suitable for time-vector analysis, and the manual nature of the method makes analysis of low-quality data (for example, noise-contaminated data) susceptible to analyst-induced biases.
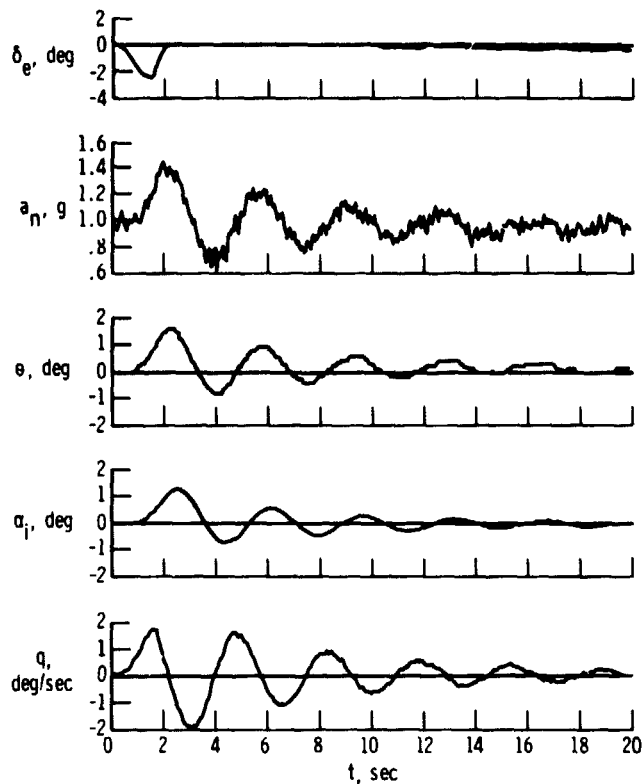
8

Figure 5. Typical time history of a longitudinal maneuver suitable for time-vector analysis. M = 2.78; h = 20,730 meters (68,000 feet).

Newton-Raphson Derivative Matching

The basic principle of the Newton-Raphson derivative determination technique (ref. 8) is the minimization of the error in matches of flight and computed time histories. Use of this method results in a complete set of stability and control derivatives, as well as a calculated time history of all parameters being matched. Lags in any of the parameters, if not taken into account, will degrade the quality of the match by interfering with the overall phasing. Appendix B presents the equations used in the Newton-Raphson technique.

In the lateral-directional mode, matching β is not required to obtain a solution, which makes this method suitable for lag determination. A Newton-Raphson match of time histories of a supersonic lateral-directional maneuver is shown in figure 6. The phase angle between the calculated and the flight angle-of-sideslip traces gives an approximation of the lag magnitude. A more accurate method of determining the lag is to compare the phase angle of the flight data, $\Phi_{(\beta_i/r)_f}$, with the phase angle, $\Phi_{(\beta_i/r)_c}$, determined from the calculated time history and assign the difference to lag in angle of attack. In this way, by comparing the flight and calculated values with a primary flight parameter, any possible overall phasing discrepancy of the match as a whole is taken into account.
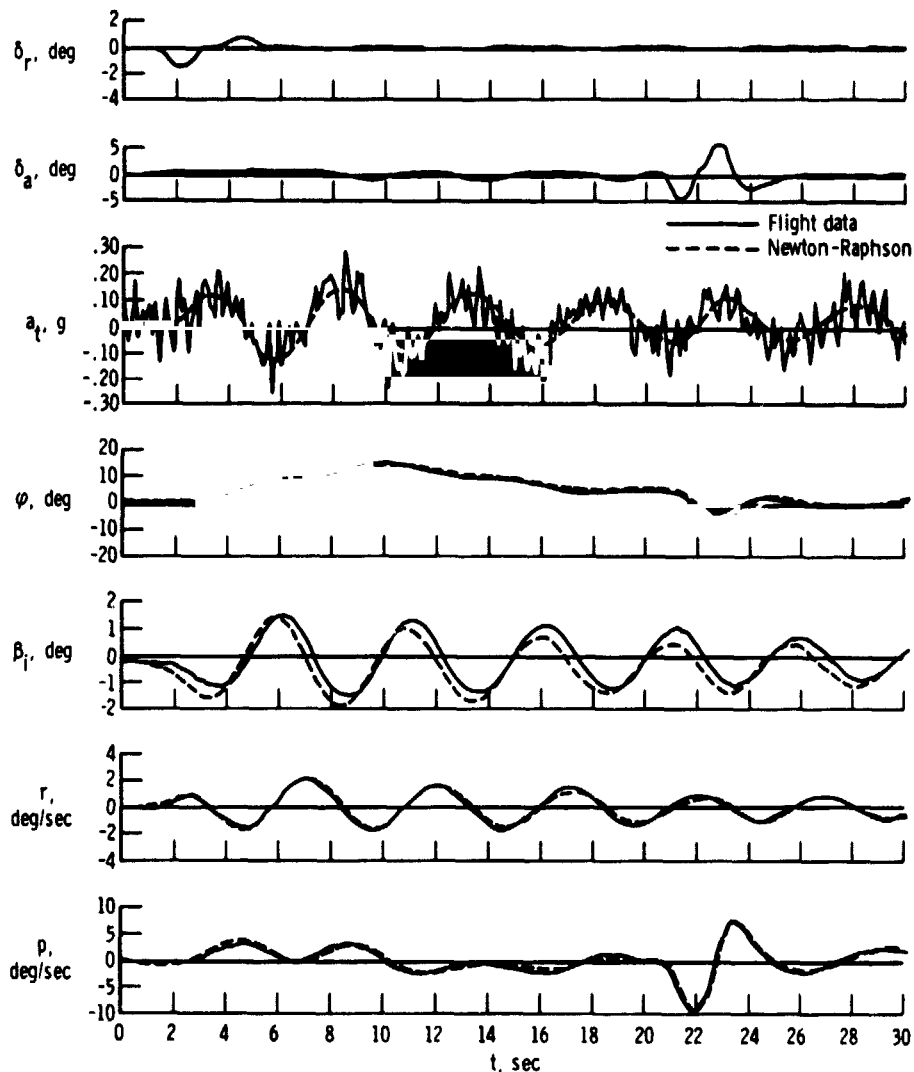
9

Figure 6. Newton-Raphson match of time histories of a lateral-directional maneuver. M = 2.76; h = 20,910 meters (68,600 feet).

Our experience has shown that the Newton-Raphson method is not well suited to determining lags in data from longitudinal maneuvers. In addition to normal acceleration, pitch rate, and pitch attitude, the angle-of-attack trace must be used to arrive at a successful Newton-Raphson match. Using the uncorrected flight α will result in a match, but the derivatives are thereby biased, and the quality of the match, as measured by the fit error of the parameter time histories, is not the best obtainable. In this instance the α trace must be adjusted for lag to obtain a reliable analysis.

Least-Squares Fit Error Minimization

The least-squares technique is a general technique in that time histories of all types of maneuvers are suitable for lag determination. Time histories of α or β

10

for a given maneuver were calculated from accelerations and angular rates using the equations in appendix C. Figure 7 presents flight and calculated time histories of two longitudinal maneuvers and one lateral-directional maneuver. Figure 7(a) presents the α traces for the longitudinal maneuver shown in figure 5, and figure 7(b) presents β for the supersonic lateral-directional maneuver shown in 'gure 6. The highly damped α response typical of subsonic longitudinal dynamics i. shown in figure 7(c).
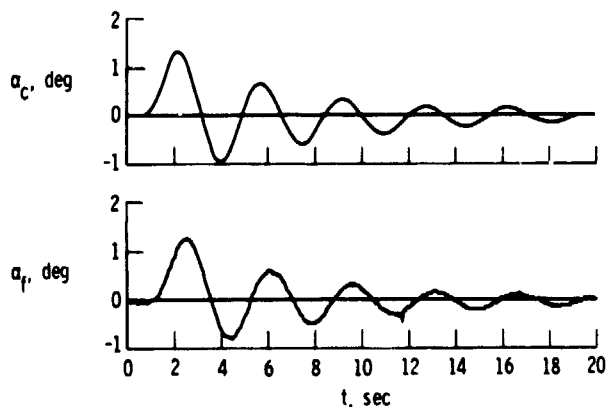
*(a) Longitudinal maneuver. M = 2.78; h = 20,730 meters (68,000 feet).*
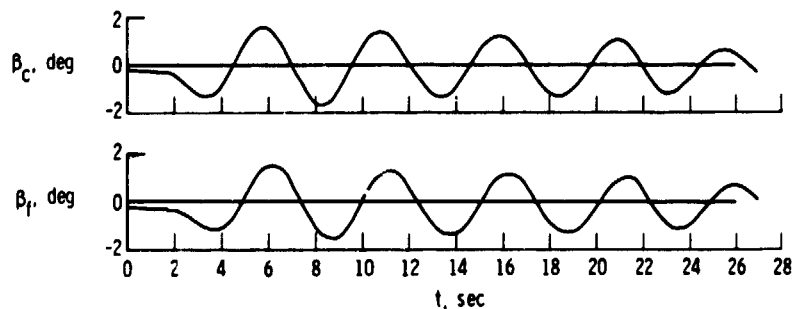
(b) Lateral-directional maneuver. M = 2.76; h = 20,910 meters (68,600 feet).
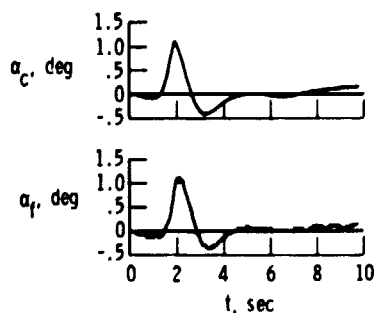
*(c) Longitudinal maneuver. M = 0.80; h = 6,460 meters (21,200 feet).*

Figure 7. Flight and calculated time histories of angle of attack and angle of sideslip for three maneuvers.

11

Plotting a calculated time history against a flight α or β trace at some chosen sample rate over the same time segment would produce a straight line if there were no time lag. The presence of a lag is shown as a phase shift between the two time histories and introduces a loop into the plot. Cross-plotting the data of figure 7 results in the ellipse type of plot shown in the upper half of figures 8(a) to 8(c). The standard deviation, σ, from a least-squares straight-line fit through the points of the loop provides a quantitative indication of the time lag.
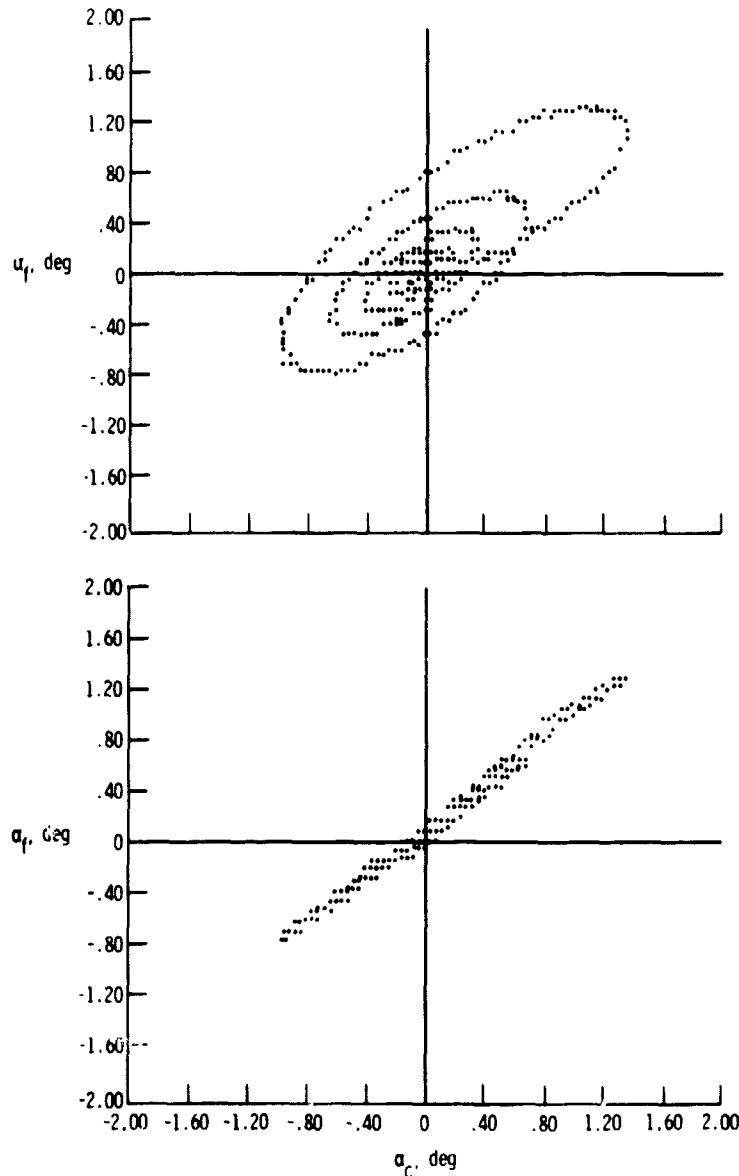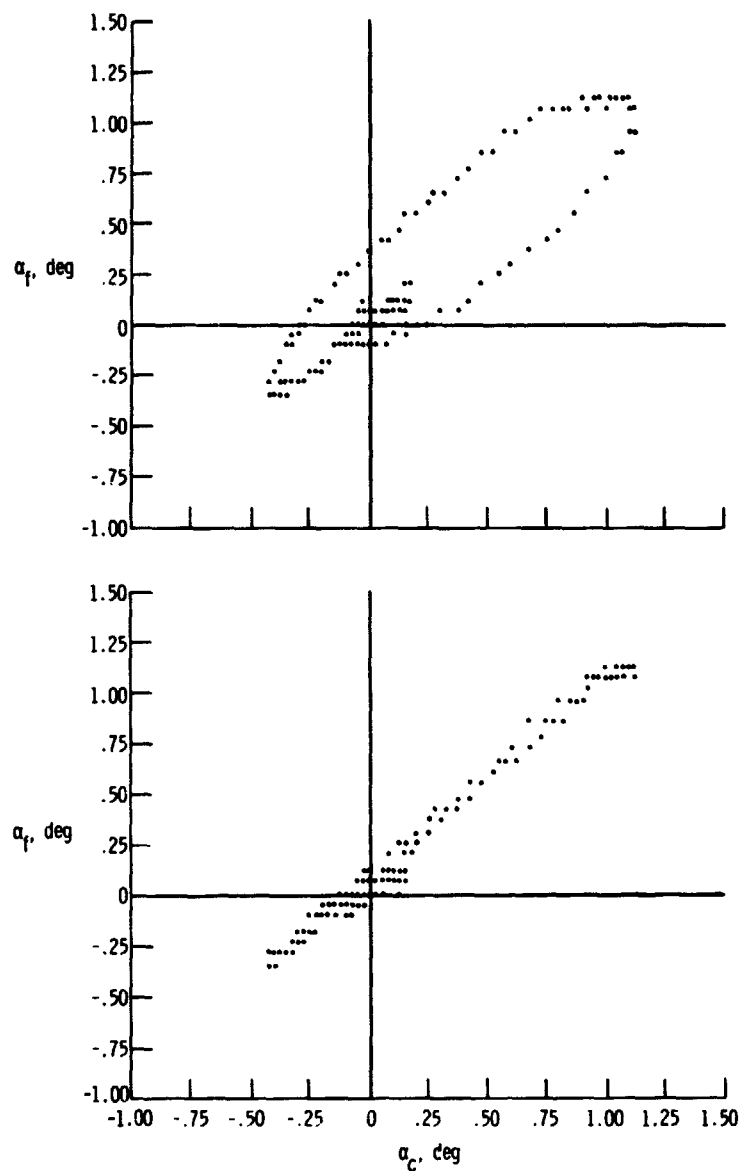

(a) Supersonic longitudinal maneuver shown in figure 7(a). Standard deviation minimized for Δt = 0.40 second.

Figure 8. Basic and time-shifted cross plots of flight and calculated angle of attack and angle of sideslip for three maneuvers shown in figure 7.
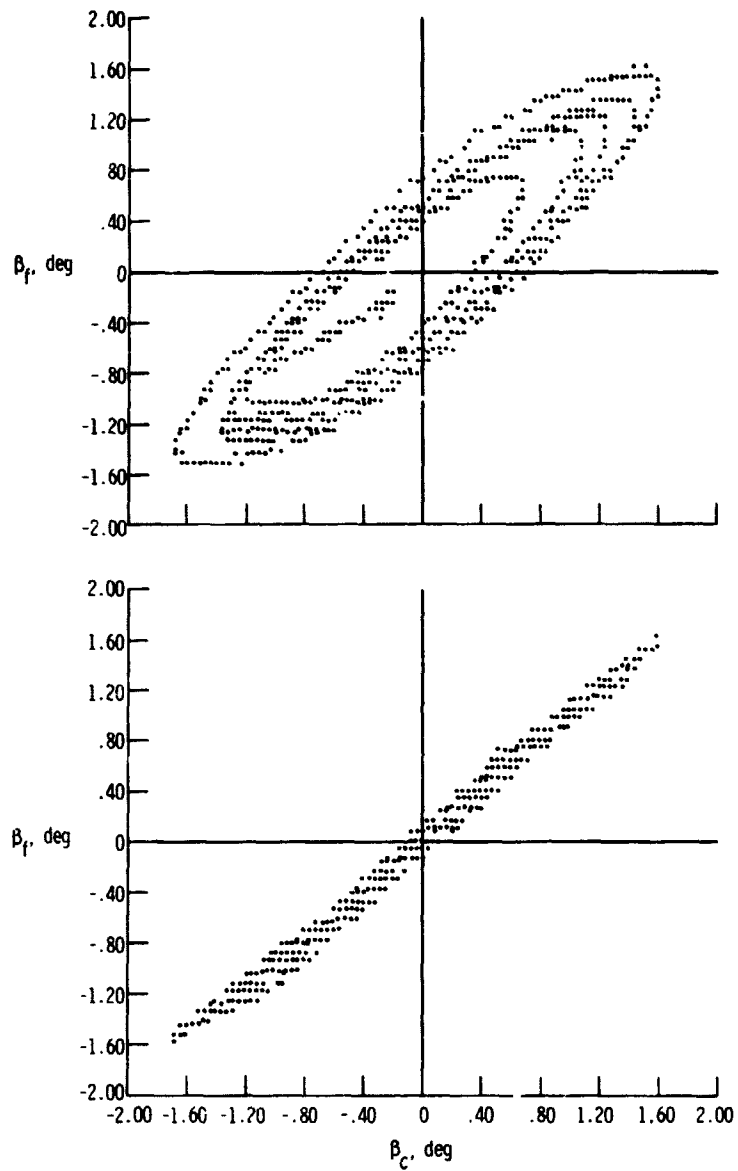
(b) Supersonic lateral-directional maneuver shown in figure 7(b).
Standard deviation minimized for Δt = 0.35 second.

Figure 8. Continued.

13

(c) Subsonic longitudinal maneuver shown in figure 7(c).
Standard deviation minimized for $\Delta t = 0.15$ second.

Figure 8. Concluded.

As the flight time history of α or β is shifted backward in time with respect to the calculated α or β, the lag is reduced and the size of the loop decreases, as shown in the lower plots of figures 8(a) to 8(c). The time shift, Δt, that minimizes σ defines the magnitude of the lag within the resolution of the chosen sample rate of 40 points per second. The trend of σ with Δt for all three maneuvers is shown in figure 9, in which the corresponding minimums of standard deviation are well defined.
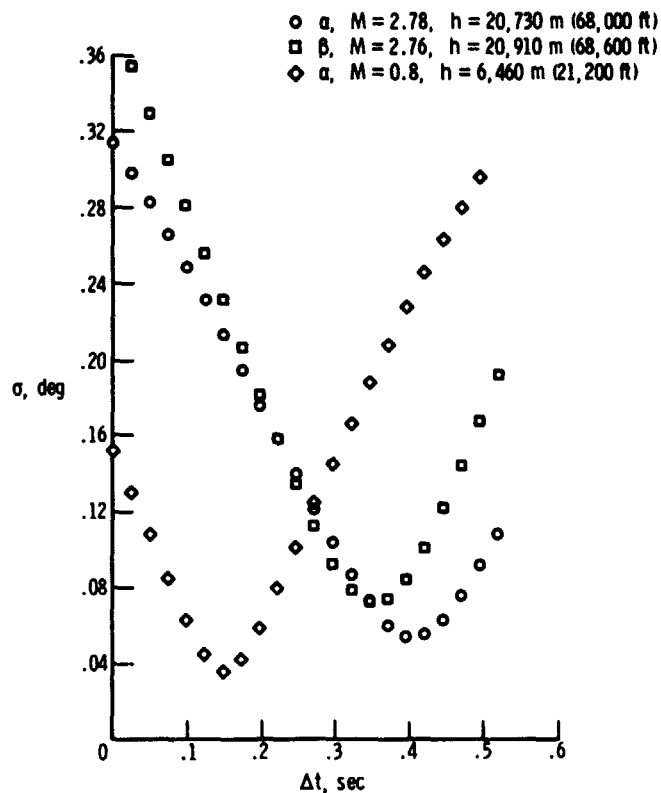
14

*Figure 9. Variation of standard deviation as a function
of time shift for the three sample maneuvers.*

Even though the least-squares method is a general technique, the best results
are obtained from analyses of highly dynamic maneuvers and maneuvers with low
effective damping.

ACCURACY

The application of the Newton-Raphson and the least-squares techniques pro-
duces solutions with minimum errors, as stated by the definition of their mathemat-
ical development. The minimum error is in turn dependent on the accuracy of the
mathematical model used and the quality of the data. An exact assessment of the
effect of model and data errors on the solution is complex and beyond the scope of
this report. However, it is estimated that the error in the measured time lag is
approximately ±0.05 second. This estimate is based on the high accuracy and fre-
quency response of the data system instrumentation, experience with stability and
control analysis using similar data systems, and a review of the lag results. It is
estimated that the combined effects of the PCM system, parameter calibration, and

various instrument characteristics produced less than 1-percent full-range error on the parameters used. In perturbation equations, such as those in this report, the constant or bias errors canceled out, and the parameter errors were less than 1 percent. Figure 9 illustrates, qualitatively, the uniqueness of the least-squares solution.

The influence of aircraft flexibility on the results was assessed and found to be negligible.

The time-vector approach requires a visual fairing of the data to obtain amplitude ratios and phase angles. Therefore, the accuracy of the results is similar to that of the Newton-Raphson and least-squares methods.

RESULTS AND DISCUSSION

Flight-Determined Lag

The α and β sensor system configurations were essentially the same; therefore, no marked difference between lag in α and β was anticipated. Lag results from all three methods are presented as a function of Mach number and knots equivalent airspeed in figures 10 to 12.

Time-vector-determined lag results are presented in figure 10 for the angle-of-attack and the angle-of-sideslip systems. An apparent increase in lag with increasing Mach number is shown; however, the increase in Mach number also generally represents increasing altitude. The data are not sufficient nor definitive enough for Mach number and altitude effects to be separated. For the α system, only supersonic data are shown because high damping precluded analysis of data from subsonic maneuvers. The scatter of the data is nominal, inasmuch as the sample rate interval was 0.025 second.
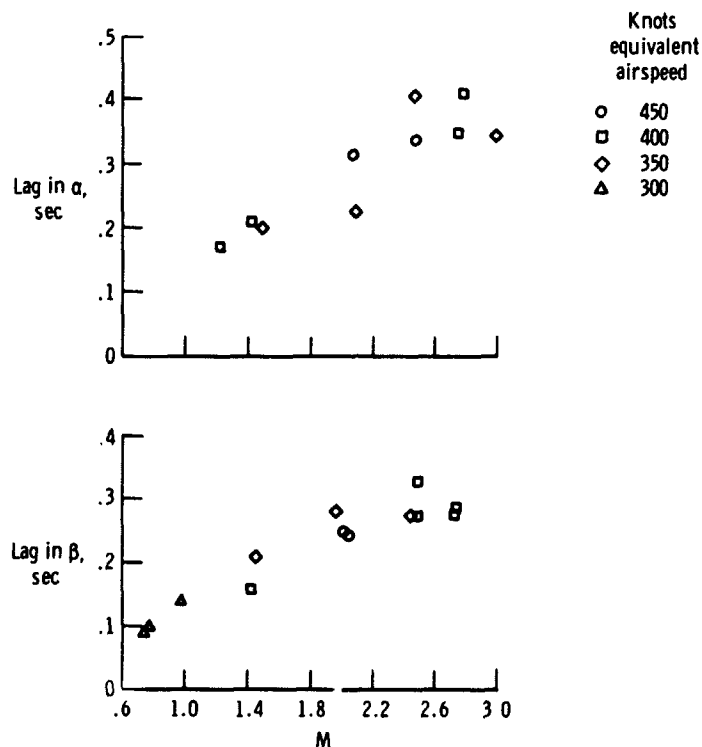
Figure 10. Lag determined by time-vector method as a function of Mach number and knots equivalent airspeed.

16

Newton-Raphson-determined lag for the β system is shown in figure 11. It was not possible to determine angle-of-attack lag with this technique because angle-of-attack matching is required to obtain consistent Newton-Raphson results. The lag trend with Mach number is similar to that obtained with the time-vector method, and the variation is approximately equal to the PCM sample rate interval.
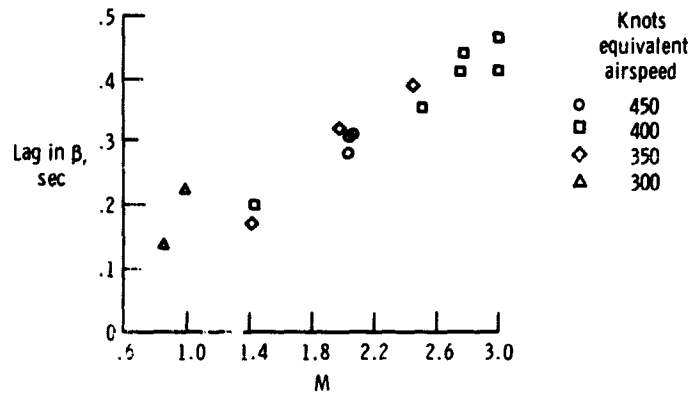

Figure 11. Lag determined from Newton-Raphson matches as a function of Mach number and knots equivalent airspeed.

Least-squares-determined lag results are shown in figure 12 for the angle-of-attack and the angle-of-sideslip systems. The trends are the same as those determined by the time-vector and Newton-Raphson techniques. There are many more
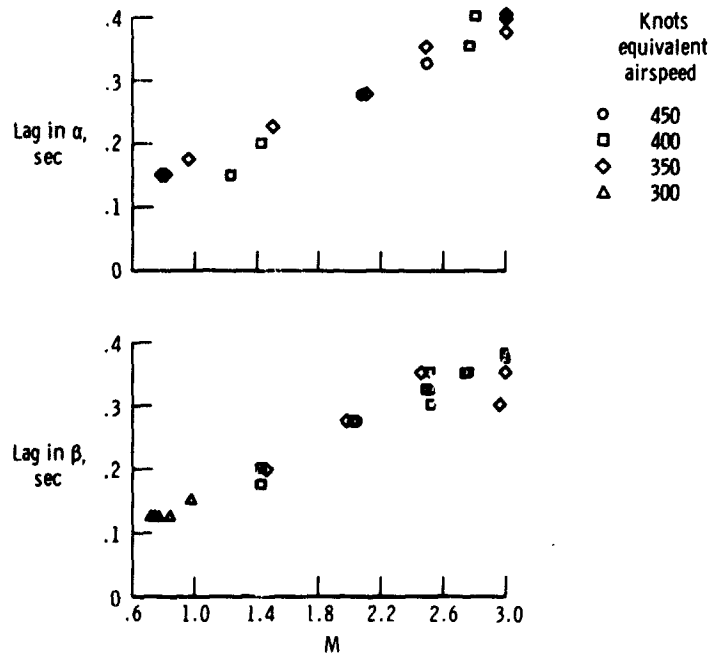

Figure 12. Lag determined by least-squares technique as a function of Mach number and knots equivalent airspeed.

data points than for the other techniques, because the general nature of the least-squares technique permits analysis of all types of maneuvers. The automatic nature of the technique eliminated analyst-induced errors and reduced data scatter.

Although all three methods produced similar results, the least-squares technique was superior because of its general applicability and the improved data consistency, thus only the results shown in figure 12 are used in the following discussion.

Conversion of Lag to Time Constants

Most literature on pressure lag assumes a first-order lag model with a Laplace transfer function of the type $\frac{1}{1 + \tau s}$, in which τ is the time constant. For meaningful comparison of the Δt lag values with existing predictions, the values must first be converted to τ, since Δt is frequency-dependent in this model. With the data available, this was done by using the following equation, developed in reference 4:

$$\tau = \left\{ \zeta \omega_n + \frac{\omega_d}{\tan\left[57.3(\Delta t)\omega_d\right]} \right\}^{-1}$$

The frequency and damping parameters are those of the oscillation and were calculated from the stability and control derivative results.

Inasmuch as altitude instead of Mach number has traditionally been considered the major correlation parameter for lag (refs. 3 and 9), a plot of the least-squares-determined time constants for α and β as a function of altitude is shown in figure 13. The Mach number for each data point is indicated. Because of the limited flight conditions under which the stability and control maneuvers were performed, Mach number and altitude are not entirely independent in these data. An apparent trend of increasing lag with increasing altitude is shown, but the correlation between Mach number and altitude makes it impossible to separate their effects on the lag.

Theoretical Time Constants

Many methods of calculating theoretical time constants of pressure sensing systems have been developed. Three methods in particular were considered in this study in attempting to correlate flight results with theory. In the first method, which could be regarded as the classical technique, the system must be represented by only one tubing segment and one transducer. The second method considered was developed by Lamb (ref. 10) and is basically an extension of the previous method in that a variety of geometrical configurations can be considered. The third method was developed by Iberall (ref. 11) and is based on oscillatory pressure theory.
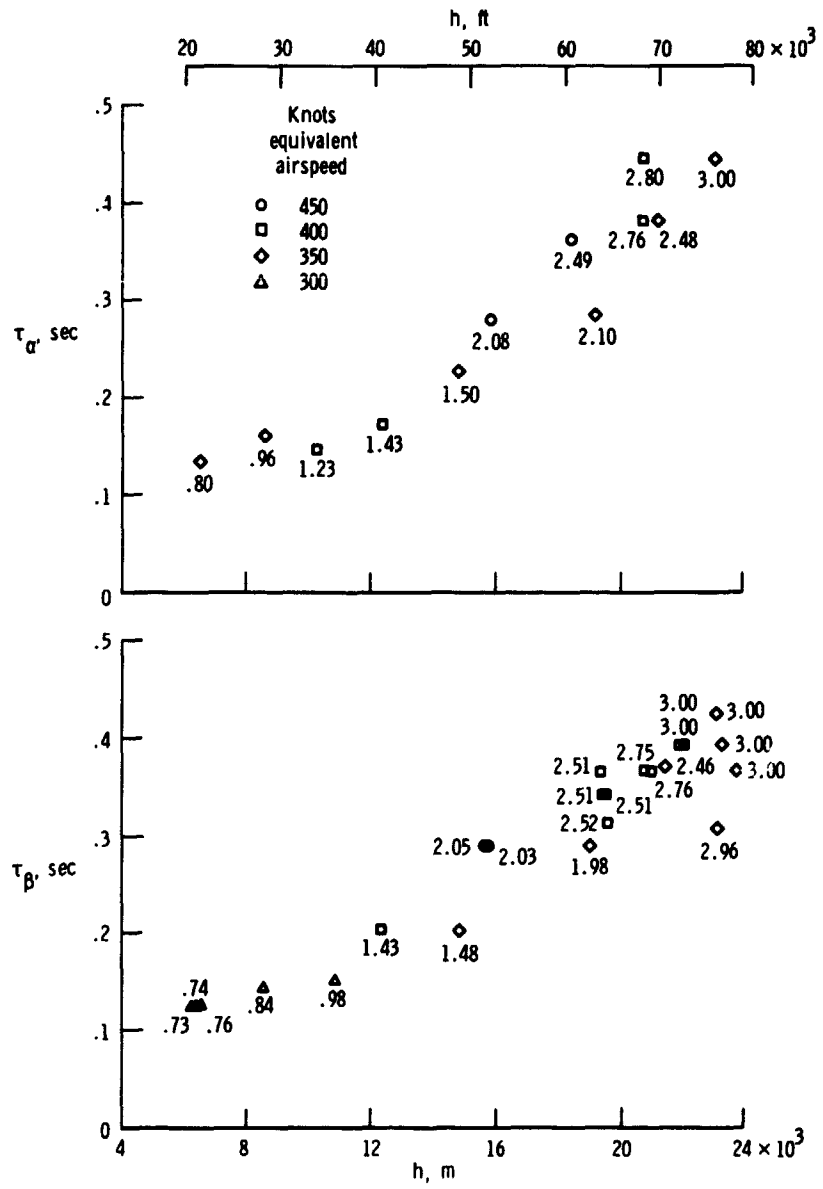
18

Figure 13. Least-squares-determined time constant plotted against altitude. Mach number is indicated for each data point.

The results from all three methods were similar for the system under consideration; therefore, only the classical theory results are presented. Spot check calculations using the other two methods were made, and the manner in which the results would differ from those of the classical theory is discussed.

In the classical theory, the time constant, τ, is proportional to the ratio of μ/P, in which μ is a function of the system temperature and P is the pressure, P_{45°, sensed at a port on the hemispherical head. Appendix D presents the method of calculating the classical theoretical time constant using only the dominant segment of tubing and the sum of the transducer volumes. Figure 14 compares the theoretical time constant of the α system with flight data. (The theoretical β system lag is 22.5 percent smaller than the α system lag.) There is essentially no agreement, because the flight-measured lags are approximately four times as great as the theoretical lags.
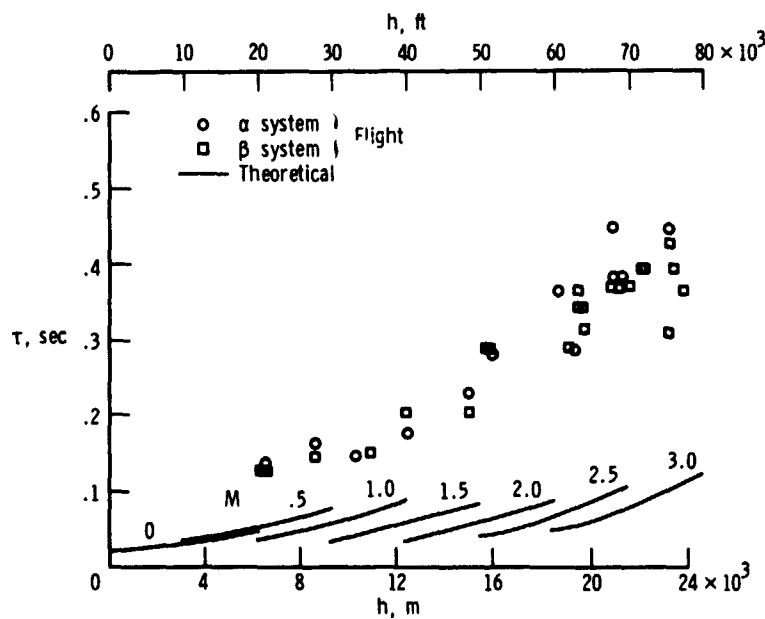

Figure 14. Comparison of flight time constants for the α and β systems with theoretical time constants of the α system.

Theoretical calculations based on the method developed by Lamb indicated that the port and the first 43.2-centimeter (17-inch) segment of tubing would increase the lag shown in figure 14 by 28 percent, which is still much lower than that for the flight data. Calculations made using the oscillatory pressure theory developed by Iberall resulted in lag values similar to those obtained by using Lamb's technique. However, it cannot be concluded that the classical theory is incorrect. The α and β system lags were calibrated in the laboratory, and the results agreed with those of the classical theory. In the laboratory, known pressure variations (primarily

ramps) were applied directly to the ports, whereas in flight the flow field around the hemispherical head determined the port pressure. The results in this report are based on dynamic maneuvers; hence α and β changed with time, which in turn caused a mass flow in and out of opposing hemispherical head ports. A primary contributor to the lag discrepancy could be the mass flow interference around the port, which in turn would affect the hemispherical head pressure field. Reference 12 discusses this flow interaction phenomenon as it relates to static-pressure measurements in climbs and descents for a typical pitot-static nose boom installation. Other factors not accounted for in the simple viscous lag theory are the dynamic flow effects of compressibility, mixed flow, and heat transfer (ref. 13).

CONCLUDING REMARKS

Flight data from the YF-12A airplane were analyzed by using three techniques to determine the magnitude of lags in the pneumatic angle-of-attack and angle-of-sideslip sensing systems over a variety of flight conditions. The techniques were applied to stability and control maneuvers and provided comparable results.

An apparent trend with Mach number showed that the lag in both sensor systems increased from approximately 0.15 second at subsonic speed to 0.4 second at Mach 3. Because Mach number was closely related to altitude for the available flight data, the individual effects of Mach number and altitude on the lag could not be separated clearly. However, the results indicated the influence of factors other than simple pneumatic lag.

Flight Research Center
  National Aeronautics and Space Administration
    Edwards, Calif., September 9, 1974

APPENDIX A

EQUATIONS FOR TIME-VECTOR ANALYSIS

The basic longitudinal equation used in time-vector analysis is

$$\dot{\alpha} = q - \frac{g}{V}(a_n - 1)$$

Expressed in time-vector format, the equation becomes

$$\omega_n \left|\frac{\alpha}{q}\right| (\Phi_{\alpha/q} + 90° + \Phi_d) = 1 - \frac{g}{V}\left|\frac{a_n}{q}\right| \Phi_{a_n/q}$$

where

$$\Phi_d = \sin^{-1}\zeta$$

The correction for probe displacement from the center of gravity is given by the equation

$$\left|\frac{\alpha}{q}\right| \Phi_{\alpha/q} = \left|\frac{\alpha_i}{q}\right| \Phi_{\alpha_i/q} + \frac{x_\alpha}{V}$$

The preceding equations are solved for the calculated $\Phi_{\alpha_i/q}$, which is then used in the expression

$$\text{Lag} = \frac{\Phi_{(\alpha_i/q)_c} - \Phi_{(\alpha_i/q)_f}}{360°} \text{ Period}$$

The basic lateral-directional equation is

$$\dot{\beta} = -r + \frac{g}{V}\varphi + p\alpha_o + \frac{g}{V}a_t$$

Expressed in time-vector format, the equation becomes

$$\omega_n \left|\frac{\beta}{r}\right| (\Phi_{\beta/r} + 90° + \Phi_d) = -1 + \frac{g}{V}\left|\frac{\varphi}{r}\right| \Phi_{\varphi/r} + \alpha_o \left|\frac{p}{r}\right| \Phi_{p/r} + \frac{g}{V}\left|\frac{a_t}{r}\right| \Phi_{a_t/r}$$

The φ/r term can be simplified by using the equations

$$\left|\frac{\varphi}{r}\right| = \frac{1}{\omega_n}\left|\frac{p}{r}\right|$$

and

$$\Phi_{\varphi/r} = \Phi_{p/r} - 90° - \Phi_d$$

The correction for probe displacement from the center of gravity is given by the equation

$$\left|\frac{\beta}{r}\right| \Phi_{\beta/r} = \left|\frac{\beta_i}{r}\right| \Phi_{\beta_i/r} - \frac{x_\beta}{V}$$

The lateral-directional equations are solved for the calculated $\Phi_{\beta_i/r}$, which is then used in the expression

$$\text{Lag} = \frac{\Phi_{(\beta_i/r)_c} - \Phi_{(\beta_i/r)_f}}{360°} \text{ Period}$$

APPENDIX B

EQUATIONS USED IN NEWTON-RAPHSON ANALYSIS

The equations of motion used to determine stability and control derivatives by the Newton-Raphson technique of matching flight and calculated data time histories are summarized in this appendix. The equations are in body-axis form.

Longitudinal Derivatives

The following equations were used to analyze longitudinal short-period maneuvers:

$$\dot{q} = M_\alpha \alpha + M_q q + M_{\delta_e} \delta_e$$

$$\dot{\alpha} = q - N_\alpha \alpha - N_q q - N_{\delta_e} \delta_e + \frac{g}{V_o}$$

$$a_n = \frac{V_o}{g} \left(N_\alpha \alpha + N_q q + N_{\delta_e} \delta_e \right)$$

$$\dot{\theta} = q$$

Position correction for instrument location was unnecessary for a_n, because the accelerometer was at the center of gravity; however, the following equation was used to correct for the α-probe location:

$$\alpha = \alpha_i + \frac{x_\alpha}{V_o} q$$

Lateral-Directional Derivatives

The analysis of lateral-directional maneuver derivatives was based on the following equations:

$$\dot{p} = \frac{I_{XZ}}{I_X} \dot{r} + L_p p + L_r r + L_\beta \beta + L_{\delta_a} \delta_a + L_{\delta_r} \delta_r$$

$$\dot{r} = \frac{I_{XZ}}{I_Z} \dot{p} + N_p p + N_r r + N_\beta \beta + N_{\delta_a} \delta_a + N_{\delta_r} \delta_r$$

24

$$\dot{\beta} = -r + \frac{g}{V_o} \varphi + p\alpha_o + Y_p p + Y_r r + Y_\beta \beta + Y_{\delta_a} \delta_a + Y_{\delta_r} \delta_r$$

$$a_t = \frac{V_o}{g} \left(Y_p p + Y_r r + Y_\beta \beta + Y_{\delta_a} \delta_a + Y_{\delta_r} \delta_r \right)$$

$$\dot{\varphi} = p + r\theta_o$$

Position correction for instrument location was not necessary for a_t because the accelerometer was at the airplane center of gravity; however, the following equation was used to correct for the β-probe location:

$$\beta = \beta_i - \frac{x_\beta}{V_o} r$$

APPENDIX C

EQUATIONS USED IN THE LEAST-SQUARES

ERROR MINIMIZATION TECHNIQUE

To calculate the α and β time histories from available accelerations and angular rates, the following two equations were used in the least-squares technique:

$$\dot{\alpha} = q - \frac{g}{V}(a_n - 1)$$

$$\dot{\beta} = -r + \alpha_o p + \frac{g}{V}(\varphi + a_t)$$

To obtain traces of α and β, the two parameters were integrated over time for the duration of the maneuver at the chosen sample rate.

Unknown parameter biases were accounted for in the analysis.

APPENDIX D

CALCULATION OF CLASSICAL THEORETICAL

TIME CONSTANT CURVES

The following representative expression for pneumatic lag in pressure instrumentation is given in reference 1:

$$\tau = \frac{32\mu(\text{Tubing length})^2}{(\text{Tubing diameter})^2\gamma P}\left[1 + \frac{\text{Instrument volume}}{(\text{Tubing length})(\text{Tubing cross-section area})}\right]$$

Most expressions of this type from other references (refs. 2 and 3, for example) follow this general form and can be summarized as:

$$\tau = K\frac{\mu}{P}$$

The constant K is some function of γ and instrument dimensions and would not change for any given installation. For the α system, $K = 10.9 \times 10^7$, and for the β system, $K = 8.44 \times 10^7$. (For this simplified analysis, only the 640-centimeter (252-inch) piece of tubing and the sum of the transducer volumes were used.) The pressure, P, is the actual pressure, P_{45°, that was sensed at the α and β ports. This port pressure was not measured; rather, the ΔP_α and ΔP_β pressures were recorded. However, wind-tunnel tests were made on the complete pitot-static and hemispherical head installation to statically calibrate the α and β measurements. Figure 15 summarizes these data as the ratio of port pressure to stagnation pressure, $\dfrac{P_{45^\circ}}{P_{t_2}}$, versus Mach number. The figure also presents some limited flight data obtained with a similar hemispherical head installation on a different airplane (ref. 14). The agreement between the flight data and wind-tunnel data is good. Also plotted is the pressure ratio obtained from modified Newtonian theory, which can be expressed as

$$\frac{P_\theta}{P_{t_2}} = \frac{P_\infty}{P_{t_2}}\sin^2\theta + \cos^2\theta$$

where $\theta = 45^\circ$.

The overall agreement of the pressure ratios in figure 15 provides confidence in the ability to calculate port pressures for the actual flight conditions of the data in this report.
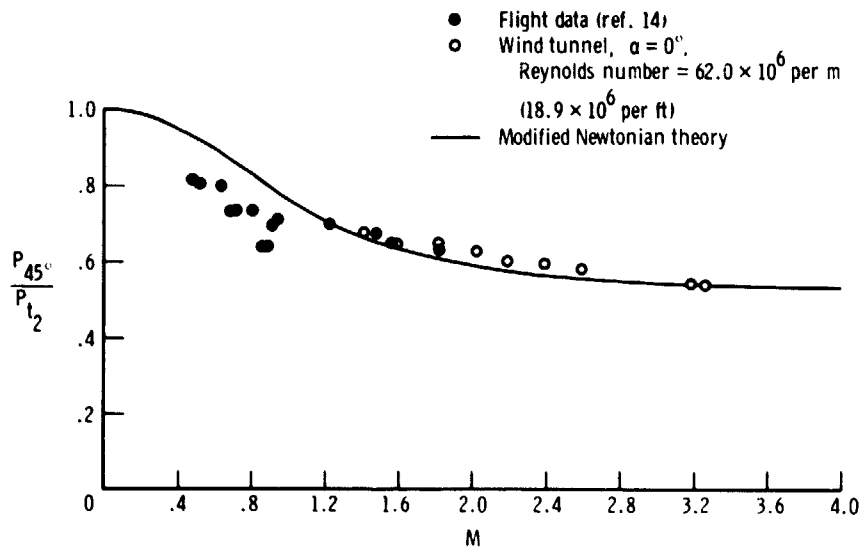
27

*Figure 15. Comparison of wind-tunnel-determined pressure
ratio with theory and flight data.*

Viscosity, μ, is a function of temperature only and can be calculated by using the following expression from reference 15:

In SI Units,

$$\mu = 145.82 \frac{T^{\frac{3}{2}}}{T + 110.4} \times 10^{-8}$$

and in U.S. Customary Units,

$$\mu = 2.270 \frac{T^{\frac{3}{2}}}{T + 198.6} \times 10^{-8}$$

However, the temperature varied throughout the tubing, so an average weighted value was necessary. Approximately 85 percent of the tubing was inside the YF-12A nose cone, which was cooled to an estimated temperature of 311° K (560° R). The temperature in the nose boom portion of the tubing ranged from the estimated 311° K (560° R) at the boom support to approximately total temperature at the stagnation point of the hemispherical head.

A theoretically precise determination of the lag was not possible because of unknown temperature gradients and the lack of actual port pressures. However, some insight into the applicability of the classical theory was obtained by calculating port pressures based on wind-tunnel and flight data and using an average weighted temperature of 333° K (600° R). Although an estimate of the temperature was used, the results were not adversely affected because lag is not extremely sensitive to temperature; for example, an increase of 56° K (100° R) would result in only a 12-percent increase in lag.

28

REFERENCES

1. Herrington, Russell M.; Shoemacher, Paul E.; Bartlett, Eugene P.; and Dunlap, Everett W.: Pressure Lag Error — Theory and Calibration. Flight Test Engineering Handbook, ch. one, sec. 4, Tech. Rep. No. 6273, Air Force Flight Test Center, May 1951 (rev. June 1964), pp. 28-47.

2. Irwin, Kirk S.: Lag in Aircraft Altitude Measuring Systems. FTC-TDR-63-26, Air Force Flight Test Center. (Available from DDC as AD 427017.)

3. Huston, Wilber B.: Accuracy of Airspeed Measurements and Flight Calibration Procedures. NACA Tech. Rep. 919, 1948.

4. Gilyard, Glenn B.; Berry, Donald T.; and Belte, Daumants: Analysis of a Lateral-Directional Airframe/Propulsion System Interaction. NASA TM X-2829, 1973.

5. Mechtly, E. A.: The International System of Units — Physical Constants and Conversion Factors. Second Revision. NASA SP-7012, 1973.

6. Montoya, Earl J.. Wind-Tunnel Calibration and Requirements for In-Flight Use of Fixed Hemispherical Head Angle-of-Attack and Angle-of-Sideslip Sensors. NASA TN D-6986, 1973.

7. Wolowicz, Chester H.: Considerations in the Determination of Stability and Control Derivatives and Dynamic Characteristics From Flight Data. AGARD Rep. 549-Part 1, 1966.

8. Iliff, Kenneth W.; and Taylor, Lawrence W., Jr.: Determination of Stability Derivatives From Flight Data Using a Newton-Raphson Minimization Technique. NASA TN D-6579, 1972.

9. Wildhack, W. A.: Pressure Drop in Tubing in Aircraft Instrument Installations. NACA TN 593, 1937.

10. Lamb, J. P., Jr.: The Influence of Geometry Parameters Upon Lag Error in Airborne Pressure Measuring Systems. Tech. Rep. 57-351, Wright Air Dev. Center, U.S. Air Force, July 1957. (Available as ASTIA Doc. No. AD 130790.)

11. Iberall, Arthur S.: Attenuation of Oscillatory Pressures in Instrument Lines. J. Res. Natl. Bur. Std., vol. 45, July 1950, pp. 85-108.

12. Silsby, Norman S.: External Interference Effects of Flow Through Static-Pressure Orifices of an Airspeed Head at Several Supersonic Mach Numbers and Angles of Attack. NASA Memo 2-13-59L, 1959.

13. Smetana, Frederick O.; and Stuart, Jay Wm., Jr.: A Study of Angle-of-Attack Angle-of-Sideslip Pitot-Static Probes. Tech. Rep. 57-234, Wright Air Dev. Center, U.S. Air Force, Jan. 1957.

14. Armistead, Katharine H.; and Webb, Lannie D.: Flight Calibration Tests of a Nose-Boom-Mounted Fixed Hemispherical Flow-Direction Sensor. NASA TN D-7461, 1973.

15. Ames Research Staff: Equations, Tables, and Charts For Compressible Flow. NACA Rep. 1135, 1953. (Supersedes NACA TN 1428.)